Cite this: DOI: 10.1039/c9fd00118b

PAPER

DNA-Driven Dynamic Assembly of MoS_2 Nanosheets

Giuseppe Amoroso,[a,b] Andrei Sapelkin,[b,c] Qingyu Ye,[a,b] Vicente Araullo-Peters,[d] Alessandro Cecconello,[a] Gustavo Fernandez[e] and Matteo Palma* [a,b]

Controlling the assembly of molybdenum disulfide (MoS_2) layers into static and dynamic superstrucutres can impact on their use in optoelectronics, energy, and drug delivery. Toward this goal, we present a strategy to drive the assembly of MoS_2 layers *via* the hybridization of complementary DNA linkers. By functionalizing the MoS_2 surface with thiolated DNA, MoS_2 nanosheets were assembled into mulitlayered superstructures, and the complementary DNA strands were used as linkers. A disassembly process was triggered by the formation of an intramolecular i-motif structure at a cystosin-rich sequence in the DNA linker, at acidic pH values. We tested the versatility of our approach by driving the disassembly of the MoS_2 superstructures through a different DNA-based mechanism, namely strand displacement. This study demonstrates how DNA can be employed to drive the static and dynamic assembly of MoS_2 nanosheets in aqueous solution.

Introduction

Transition metal dichalcogenides (TMDs) belong to an emerging class of two-dimensional (2D) layered materials with applications in diverse research areas, such as catalysis,[1,2] sensing,[3–5] energy,[6,7] and electronics.[8–10] Their general formula in chemical notation is MX_2, where M is a transition metal element (e.g. Mo or W) and X is a chalcogen atom (e.g. S, Se or Te). Among the TMD series, molybdenum disulfide (MoS_2) is the most widely studied.

A single MoS_2 nanosheet (MoS_2-NS) has a sandwich-like S-Mo-S structure, where a planar network of Mo atoms is covalently linked, in out of-plane directions, between two sheets of S atoms. Compared to the corresponding bulk material, consisting of several layers bridged by Van der Waals interactions, a single MoS_2 nanosheet exhibits a direct band gap[1,11–15] and strong photoluminescence,[11,13,14,16–18] showing promise in optoelectronic applications.[5,10,12,13,15,18] Additionally, MoS_2-NS have been employed as nanocarriers for drug delivery[19] and as laminar membranes to regulate ion transport for the desalination of seawater, toward the generation of blue energy.[6,7]

A further development in the use of MoS_2-NS for the aforementioned applications relies on the control of their surface functionalization, which directly affects their electronic properties and the distance between layers. In this regard, different strategies have been pursued to functionalize MoS_2-NS.[5,12,16,20–25] Very recently, Vera-Hidalgo *et al.* used the nucleophilic character of sulphur to functionalize MoS_2 with electrophilic maleimide derivatives at room temperature.[26] Another approach relies on the direct decoration of MoS_2-NS with thiols;[11,18,20,27,28] this has been achieved also with thiolated DNA for the formation of quantum-dot decorated MoS_2-NS,[3] and to control the assembly between MoS_2-NS for drug delivery applications.[19]

In this context, DNA is a powerful molecule for the assembly of nanoarchitectures with precise spatial arrangement,[29–36] and it has been employed in different nanomaterials, from 0D to 3D.[37,38] Moreover, DNA allows the formation of dynamic architectures, due to its ability to reconfigure, as a response to different stimuli, depending on the nucleotide sequence.[4,31] Several dynamic DNA-based nanomechanisms were demonstrated, including non-canonical base-pairing, strand-displacement, 3D motif formation and ligand−aptamer complex formation; these have further been employed in the assembly of nanostructures exhibiting a dynamic behaviour.[31,39–41]

Herein, we present a strategy for the controlled assembly of stimuli-responsive MoS_2-NS in aqueous solution, employing DNA as molecular linker. We demonstrate the functionalization of exfoliated MoS_2 nanosheets with thiol-modified DNA, and their assembly *via* DNA hybridization. Furthermore, to implement a dynamic response, MoS_2-NS were functionalized with a specific DNA sequence that reconfigures as a response to specific external stimuli. The DNA-functionalized MoS_2-NS were then assembled into multi-layered MoS_2 nanostructures *via* hybridization of the DNA complementary linkers, under basic pH conditions. The

[a] School of Biological and Chemical Sciences, Queen Mary University of London, Mile End Road, London E1 4NS, UK
[b] Materials Research Institute, Queen Mary University of London, Mile End Road, London E1 4NS, Uk
[c] School of Physics and Astronomy, Queen Mary University of London,327 Mile End Road, London, E1 4NS, UK
[d] School of Engineering and Materials Science, Queen Mary University of London,327 Mile End Road, London, E1 4NS, UK
[e] Organisch-Chemisches Institut, Westfalische Wilhelms-Universität Münster, Corrensstrasse 40, Münster 48149, Germany
Electronic Supplementary Information (ESI) available. See DOI: 10.1039/c9fd00118b

disassembly was triggered by the formation of an intramolecular i-motif structure, within the DNA tethers, at acidic pH. To demonstrate the versatility of our approach, we induced the disassembly of the DNA-linked MoS_2-NS *via* a strand-displacement mechanism. This proves the applicability of DNA linkers to drive both the assembly of MoS_2 nanosheets and to implement in their structure a dynamic molecular component.

Results and Discussion

DNA-controlled assembly of MoS_2 nanosheets

Exfoliated MoS_2-NS were obtained by sonicating MoS_2-bulk powder in aqueous sodium cholate solution (for details about the procedure, see the experimental section). The successful exfoliation of MoS_2-NS was verified spectroscopically, and through morphological characterization. Raman spectroscopy characterization (Fig. 1a) shows two strong peaks, corresponding to the in-plane vibration mode (E_{2g}^1) at 385 cm^{-1} and the out-of-plane mode (A_{1g}) of the S atoms, at 410 cm^{-1}. The MoS_2-bulk exfoliation results in the shift of the Raman peaks (see ESI Fig. 1 for Raman spectrum of MoS_2-bulk). As the number of layers decreases, the wavenumber of the E_{2g}^1 mode shifts to higher frequencies and the wavenumber of the A_{1g} mode shifts to lower frequencies. In the optical absorption spectrum, the presence of the four peaks further confirms the band structure of exfoliated MoS_2-NS (Fig. 1b): The A and B peaks, characteristic for MoS_2 dispersions, arise from the interband excitonic transitions at the K point of the Brillouin zone, while the C and D peaks can be assigned to the direct excitonic transition of the M point. In addition, transmission electron microscopy (TEM) imaging for the exfoliated MoS_2 nanosheets indicates that the samples exhibit a sheet-like structure (Fig. 1c).

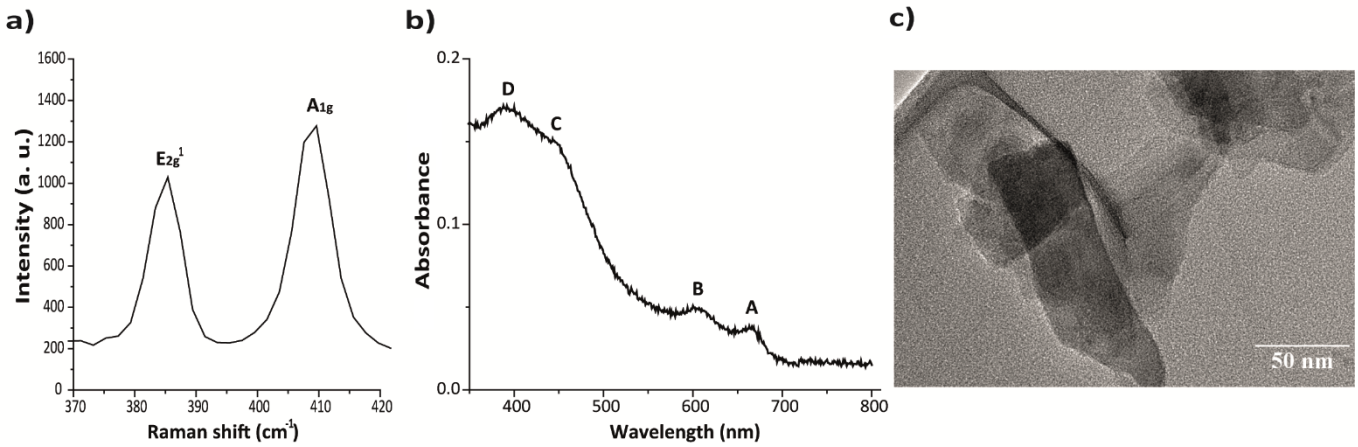

Fig. 1 Exfoliated MoS_2-NS obtained by sonicating MoS_2-bulk powder in aqueous sodium cholate. (a) Raman spectrum showing the typical in-plane vibration mode (E_{2g}^1) at 385 cm^{-1} and the out-of-plane vibration mode (A_{1g}) of the S atoms, at 410 cm^{-1}; (b) UV-vis absorption spectrum where the four peaks confirm the band structure of exfoliated MoS_2-NS: The A and B peaks, at 666 nm and 605 nm respectively, characteristic for MoS_2 dispersions, arise from the interband excitonic transitions at the K point of the Brillouin zone, while the C and D peaks, at 450 nm and 395 nm respectively, can be assigned to the direct excitonic transition of the M point; (c) representative TEM image of the starting material of this study: MoS_2-NS.

In order to drive their assembly, MoS_2 nanosheets were first functionalized with DNA sequences (**1**) and (**2**) (for details, see the experimental section and ESI Fig. 2). The as-prepared MoS_2-NS solution was divided in two aliquots: DNA sequence (**1**) was added to the first aliquot, and DNA sequence (**2**) to the second one. DNA sequences (**1**) and (**2**) are thiolated DNA strands that can be anchored to the intrinsic sulphur defects on MoS_2-NS surfaces. This functionalization process produces (**1**)-functionalized MoS_2-NS, **M1**, and (**2**)-functionalized MoS_2-NS, **M2**.

To verify the functionalization of MoS_2-NS, the concentration of DNA in **M1** and **M2** was estimated by spectrophotometry (see ESI Fig. 3 for details). Readings were taken at 260 nm and the concentration of DNA strands (**1**) and (**2**) was found to be 0.54 µM and 0.65 µM, respectively, for **M1** and **M2**; these values were used to estimate the number of DNA strands per MoS_2-NS, which resulted to be 61 in **M1** and 73 in **M2** (see experimental section). **M1** and **M2** were then mixed together in a solution containing 400mM NaCl and 2 mM MOPS (3-(N-morpholino)propanesulfonic acid), and the MoS_2-NS were assembled *via* DNA hybridization of the complementary strands **(1)** and **(2)**, as shown in Fig. 2a, resulting in the hybrid structure **M1/M2**. The Raman spectrum of **M1**/**M2** (Fig. 2b) shows that the E_{2g}^1 peak shifted to lower frequencies as well as the A_{1g} peak shifted to lower frequencies compared to the MoS_2-NS Raman peaks shown in Fig. 1a.

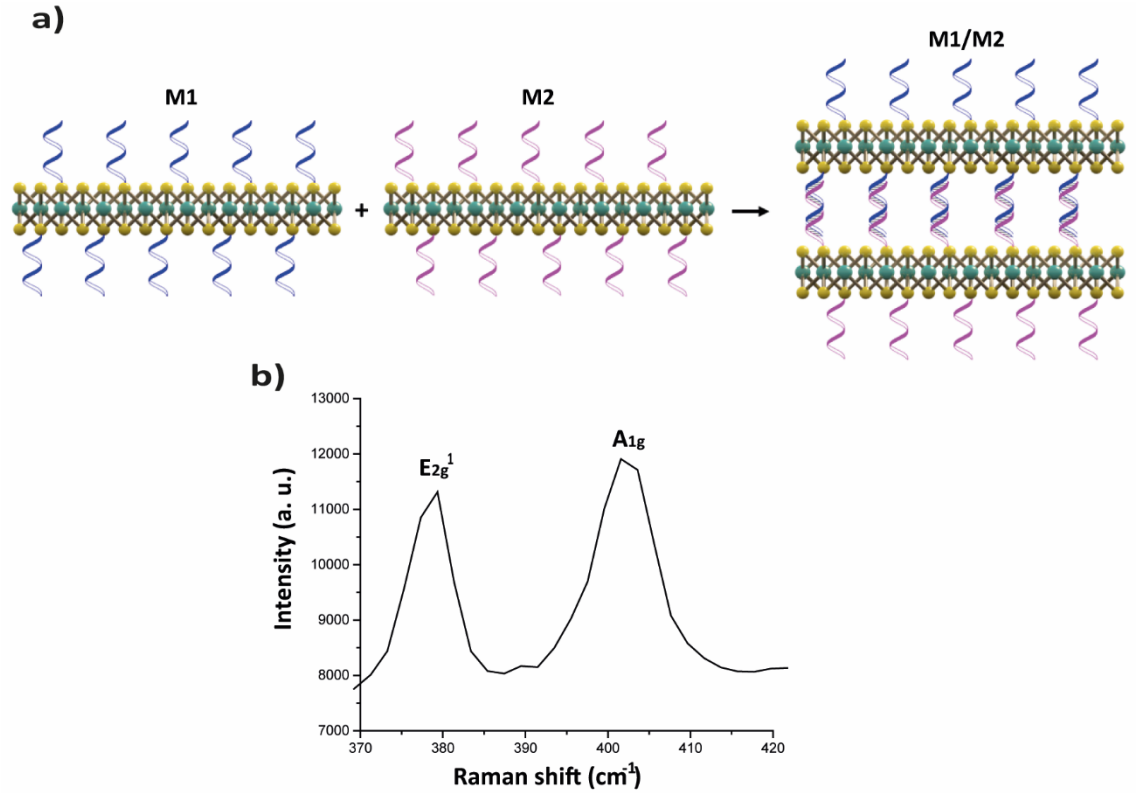

Fig. 2 Formation of DNA-linked MoS_2 nanosheets *via* DNA hybridization. (a) Scheme of the assembly, (b) Raman spectrum showing that the E_{2g}^1 peak shifted to lower frequencies, 379 cm^{-1}, as well as the A_{1g} peak shifted to lower frequencies, 402 cm^{-1}, compared to MoS_2-NS Raman peaks shown in Fig. 1a.

To demonstrate the successful assembly of **M1**/**M2**, Atomic Force Microscopy (AFM) characterization was carried out on samples obtained by casting MoS_2-NS on muscovite mica. Fig. 3 shows the corresponding AFM topographical images and the height profiles of MoS_2-NS and DNA-linked MoS_2 nanosheets physisorbed on mica. The lateral size and thickness of the starting MoS_2-NS were found to be 94.9 ±26.9 nm and 5.3 ±2.1 nm, respectively, corresponding to an average number of nanosheets per structure equals to 8 ±3 MoS_2 monolayers. DNA-linked MoS_2 nanosheets display a width of 129.6 ± 53.1 nm and a height of 17.9 ± 7.0 nm, suggesting that the superstructures consist of an average number of monolayers equal to 29 ±11, and that the assembly of MoS_2 nanosheets has taken place. Additionally, to confirm that MoS_2-NS can assemble only when functionalized with complementary DNA strands, we carried out a morphological characterization of samples obtained by casting solutions of MoS_2-NS functionalized with DNA strands that cannot form a duplex. Fig. 4a, in the ESI, shows that the measured height of the MoS_2-NS is comparable to that obtained for the starting material, hence indicating that no assembly has taken place. In a similar way, if an amino-modified DNA strand (**2**) incapable of functionalizing MoS_2-NS is employed, no evidence of assembly was observed (see ESI Fig. 4b).

Stimuli-responsive DNA-functionalized MoS_2 nanosheets

In order to use the ability of DNA to induce a stimuli responsive behaviour in DNA-linked nanostructures,[39,40] we introduced a cytosine-rich DNA sequence, (**3**), and its partly complementary strand **(2)**, as the molecular linkers of choice in the assembly of MoS_2 NS (see the experimental section for details). Sequence (**3**) is capable to reconfigure in response to a pH change in the buffer solution. For this purpose, we functionalized MoS_2-NS with thiol modified (**3**), forming (**3**)-functionalized MoS_2-NS, **M3**. The concentration of DNA in **M3** was estimated by UV-vis analysis (see ESI Fig. 5 for details) and it was found to be 0.71 μM, while 80 DNA strands were estimated to be present per MoS_2-NS, for **M3** (see experimental section). Upon mixing of **M2** and **M3** at basic pH, DNA sequence (**3**) hybridizes with its complementary DNA (**2**) forming a partial DNA duplex (**2**)/(**3**), leading to the assembly of **M2** and **M3**. When the pH of the buffer is changed to acidic conditions, (**3**) forms a four-stranded intramolecular quadruplex structure, named i-motif.[42] The formation of this secondary DNA structure, allows the disassembly of **M2** and **M3**, as shown in Fig. 4a. For the Raman characterization of **M2**/**M3** structures at pH 8 and pH 5.5 see Fig. 6, in the ESI.

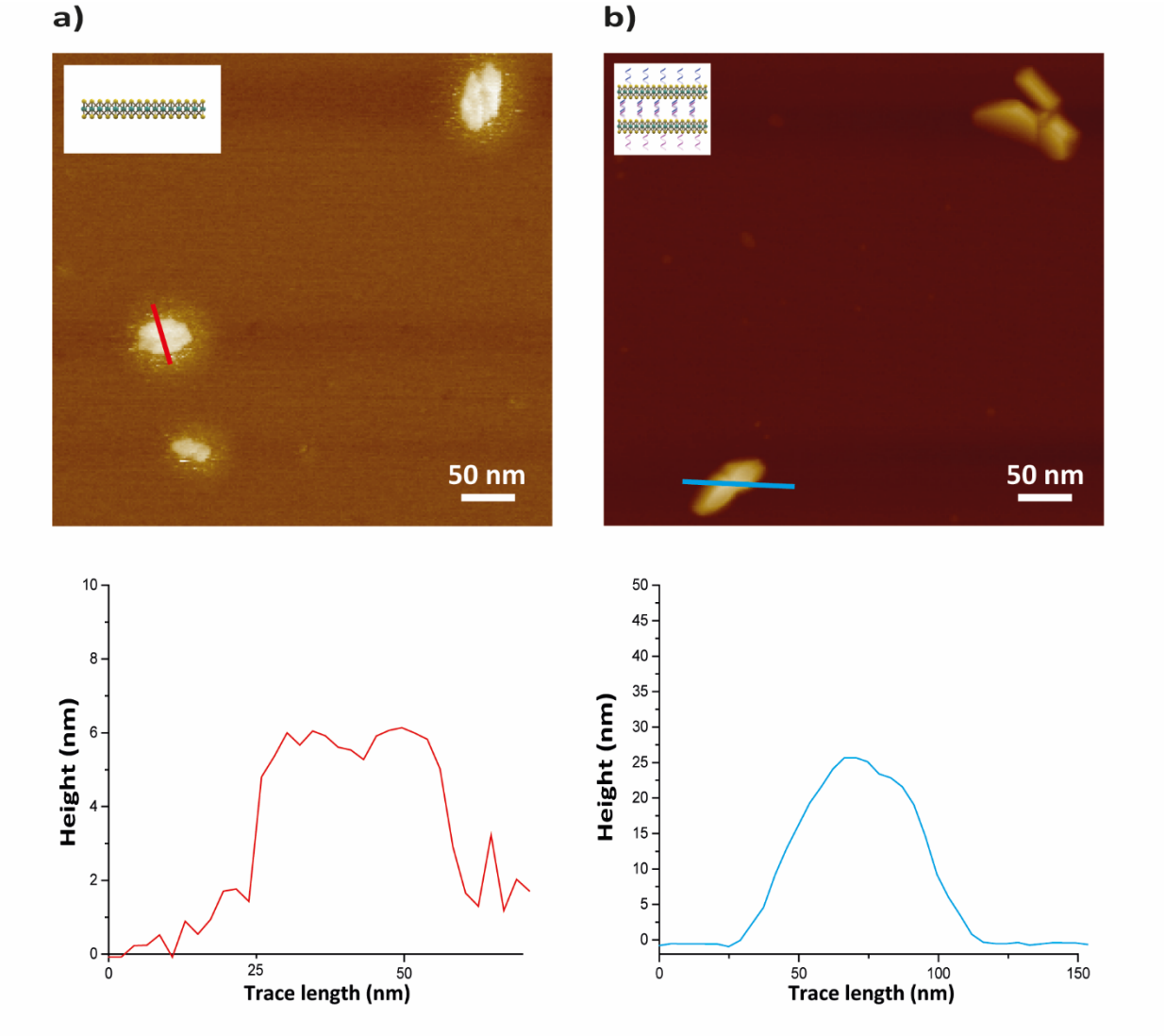

Fig. 3 (a) AFM topographical image and respective height profile of the starting material: DNA-functionalized MoS_2-NS. (b) AFM topographical image and respective height profile of DNA-linked MoS_2-NS superstructures assembled *via* DNA hybridization.

To confirm the nanosheet disassembly as a result of the pH change, we compared the size of the assembled **M2**/**M3** nanostructures with the corresponding disassembled **M2** and **M3** nanostructures. This was done *via* AFM topographical imaging of solutions cast on mica (Fig. 4b and 4c, and cross-section analyses Fig. 4d and 4e). The DNA-linked MoS_2 nanosheets, exhibit a lateral size and thickness of 338.2 ±117.7 nm and 40.4 ±18.9 nm, respectively, suggesting that they consist of an average number of monolayers equal to 65 ± 30. Differently, the lateral size and height of the corresponding disassembled MoS_2-NS, were found to be 144.8 ± 88.1 nm and 5.4 ± 3.3 nm, respectively, in line with the presence of an average number of monolayers equal to 9 ±5, i.e. comparable to the starting MoS_2-NS, prior to any DNA-driven assembly. This difference in height strongly suggests that the disassembly of the MoS_2 nanosheets can indeed be controlled by employing a specific DNA sequence capable of forming an i-motif structure at pH 5.5.

To further explore the versatility of our approach, we induced the disassembly of **M2**/**M3** *via* strand-displacement (see scheme in Fig. 5a).[43] Upon introduction of strand **(4)**, the partial duplex (**2**)/(**3**) is separated, to form the more stable duplex **(2)/(4)**, resulting in the release of strand **(3)** in solution (see the experimental section for details), and leading to the disassembly of **M2**/**M3** nanostructures into isolated **M2** and **M3** nanosheets (see ESI Fig. 7 for Raman characterization). The disassembly was verified by statistical analysis of the average MoS_2 height and length as measured *via* AFM (see Fig. 5b, c): the width and thickness of the disassembled **M2** and **M3** structures, were found to be 101.6 ±52.4 nm and 11.3 ±5.7 nm, respectively, suggesting that these structures consist of an average number of monolayers equal to 18 ± 9 MoS_2.

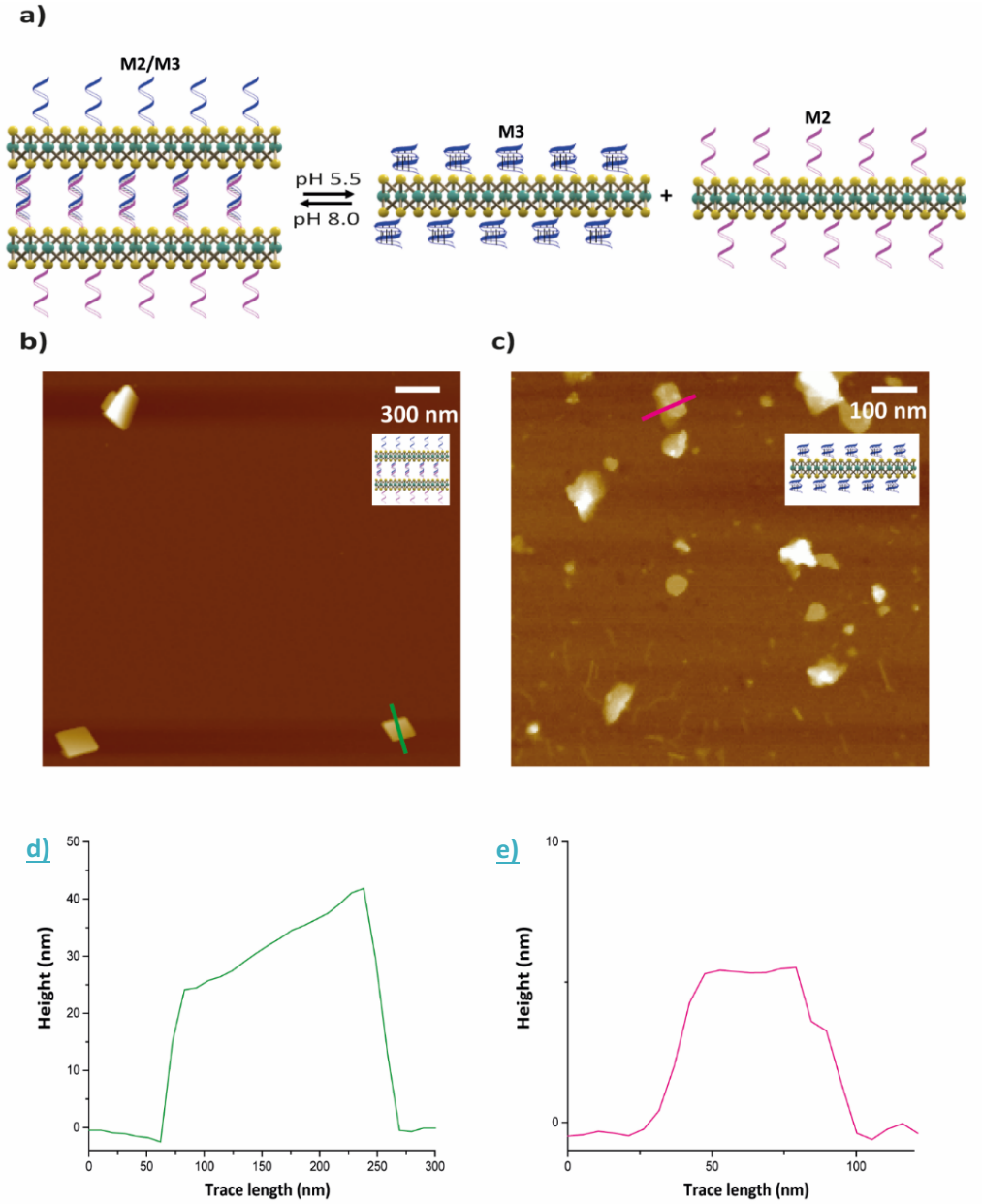

Fig. 4 Controlled disassembly of DNA-linked MoS_2 nanosheets by i-motif formation: (a) scheme of the pH-driven disassembly; (b) AFM topographical image of the assembled MoS_2 nanosheets; (c) AFM topographical image of the disassembled MoS_2 nanosheets; (d) height profile of the assembled MoS_2 nanosheets;(e) height profile of the disassembled MoS_2 nanosheets.

The difference in thickness indicates that a disassembly of the DNA-linked MoS_2 nanosheets can take place employing an additional DNA sequence capable of destabilizing the (**2**)/(**3**)-linker joining the MoS_2-NS. This strategy exhibited a lower efficiency compared to the aforementioned approach employing the i-motif strand (Fig. 4), likely due to the limited access of DNA strand **(4)** the duplex **(2)/(3)** located between the nanosheets. Finally, to prove that the disassembly occurs only when a fuel DNA strand is employed, we performed the same experiment using DNA sequence (**I**), incapable of displacing (**2**) in the DNA duplex joining **M2/M3.** Figure 8, in the ESI, shows that the disassembly does not take place in this case.

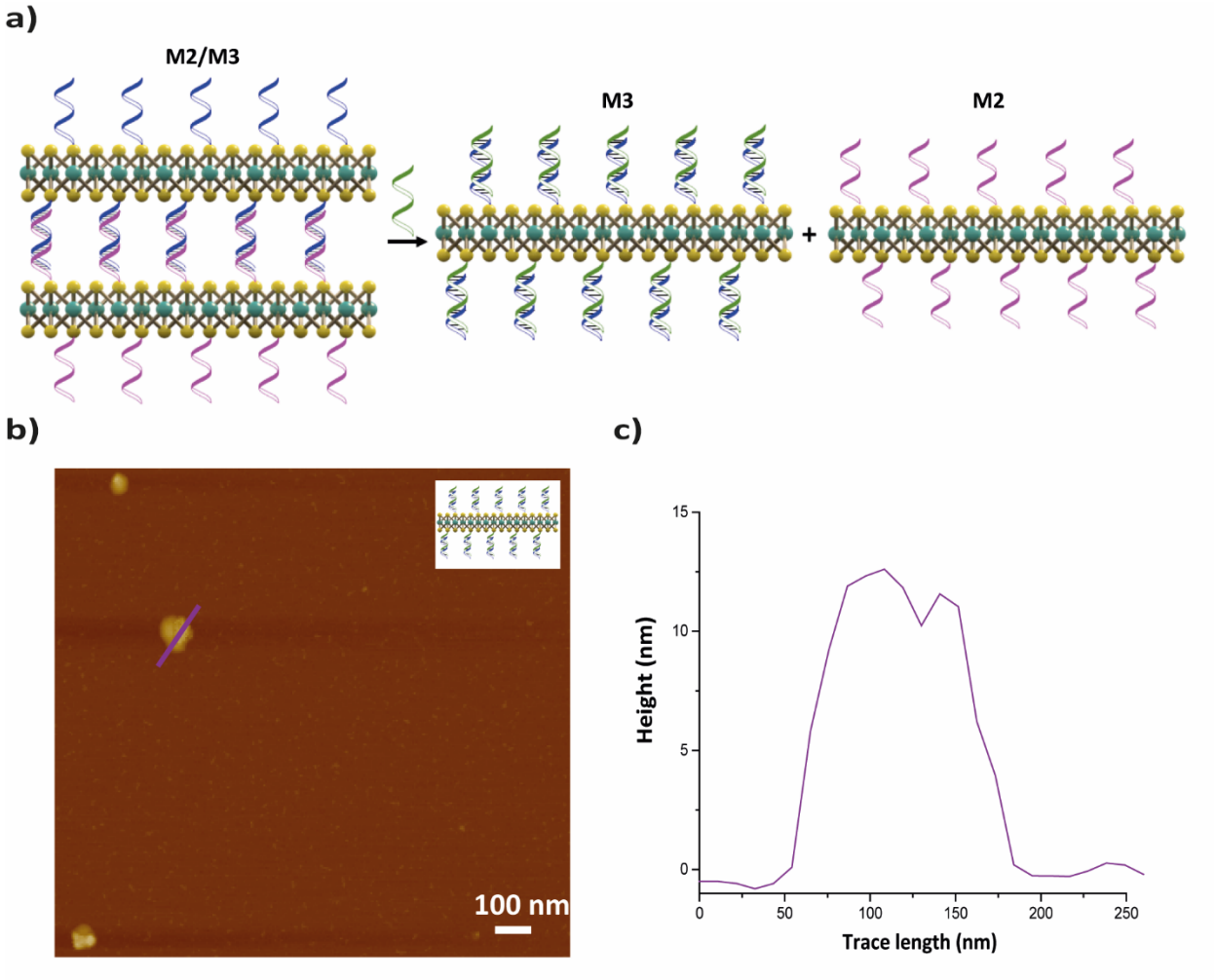

Fig. 5 Controlled disassembly of DNA-linked MoS_2 nanosheets *via* a strand-displacement mechanism (SD): (a) Schematic of the disassembly process *via* SD; (b) AFM topographical image of MoS_2 nanosheets disassembled *via* SD, and (c) corresponding height profile.

Experimental

Preparation of MoS_2 Nanosheets

MoS_2 nanosheets were obtained by exfoliation of MoS_2-bulk powders in aqueous solution. 1mL aqueous solution containing MoS_2-bulk powder (5 mg/mL; Sigma-Aldrich) and sodium cholate (1.5 mg/mL; Sigma-Aldrich) was sonicated for 24 hours at a power of 3W (Sonics, VC130PB). After sonication, the black dispersion was centrifuged at 3000 × g and the yellow supernatant collected. Then, the supernatant was centrifuged at 4000 × g and the sediments were re-dispersed in 1 mL of deionized water. This washing process was repeated three times in order to remove the sodium cholate absorbed on MoS_2 nanosheets.

DNA-functionalization of MoS_2 Nanosheets

5'-thiolated DNA oligos ordered from IDT are shipped in their oxidised form. Therefore they require a reduction process to remove the protecting group before they are used. The reducing process employed in our approach is a TCEP (Tris[2-carboxyethyl] phosphine) treatment, which consists in incubating for two hours an aqueous solution containing 10 mM TCEP and 100 µM thiolated DNA oligos at room temperature.

To functionalize the MoS_2 surface with the thiol-modified DNA, 20 µL MoS_2-NS solution were mixed with 2 µL DNA solution (100 µM) and diluted into 200 µL of buffer solution (1 × TAE; Invitrogen™). The resulting solution was then sonicated for 1 min and

incubated for 5 h at room temperature. To remove the excess of DNA, the solution was then centrifuged at 4000 × g for 30 min and the sediments re-dispersed in 100 µL of deionized water.
The number of DNA strands attached for every sulphur atom was calculated to be: $4.3 \cdot 10^{-5}$ in **M1**, $5.16 \cdot 10^{-5}$ in **M2** and $5.65 \cdot 10^{-5}$ in **M3**. The molecular weight (MW) of MoS_2 is 160.07 g/mol, while the MWs of the DNA sequences employed for the functionalization are 13,093.8 Da, 10,532.1 Da and 10,178.9 Da, respectively for thiol-(**1**), thiol-(**2**) and thiol-(**3**). The number of DNA strands attached per MoS_2-NS was estimated by assuming MoS_2-NS as a geometric cylinder with a density of 5.06 g/mL.
DNA sequences used in this study:

(**1**)= 5'-Thiol- TTT TTT TTT TTT CAC AAT CAC AAT CAC AAT CAC AAA AAA AAA -3'

(**2**)= 5'-Amino- or Thiol- TTT TTT TTT TTT GTG ATT GTG ATT GTG ATT GTG -3'

(**3**)= 5'-Thiol- TTT TTT TTT TTT CCC AAT CCC AAT CCC AAT CCC -3'

(**4**)= 5'- TGG TGG GAT TGG GAT TGG GTG GTA TA -3'

(**I**)= 5'- ACA AGA AAG CAA GCA AAT CAG ATA ACA GCC ATA TTA TTT ACC TGA GCC TGC TGC ATA -3'

DNA-linked Assembly of M1 and M2

In order to assemble MoS_2-NS, equal amounts of **M1** and **M2** solutions were combined in a buffer solution, containing MOPS (2mM; Sigma-Aldrich) and NaCl (400mM; Fisher Scientific™). The mixture was then incubated and gently shaken for 1 h.

Stimuli-responsive Assembly of M2 and M3

To drive the assembly of MoS_2-NS at basic pH, a solution containing 2mM MOPS, 400 mM NaCl, and equal amounts of **M2** and **M3** at pH 8, was incubated and shaken for 1 h. In order to induce the acidic pH-stimulated disassembly, the pH of the **M2**/**M3** solution was adjusted to 5.5 by adding 1 mM HCl and incubated for 30 min at 25°C. Disassembly of **M2**/**M3** into isolated **M2** and **M3**, *via* strand displacement was achieved by adding DNA strand (**4**) at a final concentration of 30 µM.

Raman Spectroscopy

2 µL sample solutions were drop-cast on clean silicon wafers (Silicon Quest International, Inc). The samples were then allowed to dry under air at room temperature and characterized by Raman spectroscopy. Raman analysis of the samples was carried out on a Renishaw inVia confocal Raman microscope. Raman spectra were measured using 442 nm laser line.

UV-Vis Spectroscopy

Optical absorption measurements were carried out on a Cary 100 UV-Visible Spectrophotometer from Agilent Technologies.

TEM

10 µL sample solutions were drop-cast on a Holey Carbon Films 400 Mesh Copper Grid (Agar Scientific Ltd), air-dried at room temperature in a clean fume hood, and characterized by TEM. TEM imaging of the samples was carried out on a Jeol JEM 1230 TEM equipped with a Morada CCD camera and iTEM software.

AFM

20 µL sample solutions were drop-cast on freshly cleaved muscovite mica discs (Agar Scientific), pre-treated with $MgCl_2$ solution (1 M, Sigma Aldrich), incubated for 30 min and characterized by AFM. AFM analysis of the samples was carried out on a Bruker Dimension Icon in PeakForce Tapping mode with ScanAsyst Air tips from Bruker. Lateral size and thickness analysis were obtained by Image-J 1.51j8 and NanoScope Analysis 1.5 software, respectively.

Graphics

Graphics plots were generated by OriginPro 2015 (V b9.2.257).

Conclusions

We demonstrated a strategy to drive the assembly of MoS_2-NS and their disassembly under different stimuli. MoS_2-NS were functionalized with thiolated-DNA strands, using the sulphur vacancies in the exfoliated nanosheets, and then assembled *via* base-complementary of the DNA sequences. The successful assembly was verified by AFM morphological characterization, comparing the heights of MoS_2-NS and assembled MoS_2-NS. Furthermore, we demonstrated the disassembly of DNA-linked MoS_2-NS by changing the pH of the solution. This was achieved by employing a cytosine-rich DNA sequence that reconfigures into an intramolecular i-motif structure at acidic pH, and separates the DNA duplex linking the MoS_2-NS. Finally, we tested the versatility of our approach by driving the disassembly of the DNA-linked MoS_2-NS *via* a strand-displacement mechanism. The strategy

presented in this study is of interest for controlling the static and dynamic assembly MoS_2-NS in aqueous solution, and can be used for optoelectronic and biotechnology applications, as well as for the assembly of 2D materials into laminar membranes.

Conflicts of interest

There are no conflicts of interest to declare.

Acknowledgements

The authors gratefully acknowledge financial support from the Air Force Office of Scientific Research under award FA9550-17-1-0179. G.A. is financially supported by the Materials Research Institute of Queen Mary University of London and the Westfälische Wilhelms University of Münster (WWU). Q.Y. is financially supported by the China Scholarship Council. A.C. is supported by a fellowship of the Federation of European Biochemical Societies (FEBS).

References

1 D. Voiry, J. Yang, M. Chhowalla, *Adv. Mater.*, 2016, **28**, 6197-6206.
2 J. Kibsgaard, Zhebo Chen, Benjamin N.Reinecke and Thomas F.Jaramillo, *Nat. Mater.*, 2012, **11**, 963-969.
3 F. Bian, L. Sun, L. Cai, Y. Wang, Y. Zhao, S. Wang and M. Zhou, *Biosens. Bioelectron.*, 2019, **133**, 199-204.
4 W. Ji, D. Li, W. Lai, X. Yao, M. F. Alam, W. Zhang, H. Pei, L. Li and A. R. Chandrasekaran, *Langmuir*, 2019, **35**, 5050-5053.
5 Y. Zhao, S. Ippolito and P. Samorì, *Adv. Opt. Mater.*, 2019, **7**, 1900286.
6 Y. Kang, Y. Xia, H. Wang and X. Zhang, *Adv. Funct. Mater.*, 2019, **29**, 1902014.
7 W. Li, Y. Yang, J. K. Weber, G. Zhang and R. Zhou, *ACS Nano*, 2016, **10**, 1829-1835.
8 Q. H. Wang, K. Kalantar-Zadeh, A. Kis, J. N. Coleman and M. S. Strano, *Nat. Nanotechnol.*, 2012, **7**, 699-712.
9 M. Osada and T. Sasaki, *J. Mater. Chem.*, 2009, **19**, 2503-2511.
10 S. Witomska, T. Leydecker, A. Ciesielski and P. Samorì, *Adv. Funct. Mater.*, 2019, **29**, 1901126.
11 D. M. Sim, M. Kim, S. Yim, M. J. Choi, J. Choi, S. Yoo and Y. S. Jung, *ACS Nano*, 2015, **9**, 12115-12123.
12 A. Hirsch and F. Hauke, *Angew. Chemie - Int. Ed.*, 2018, **57**, 4338-4354.
13 H. Li, Q. Zhang, C. C. R. Yap, B. K. Tay, T. H. T. Edwin, A. Olivier and D. Baillargeat, *Adv. Funct. Mater.*, 2012, **22**, 1385-1390.
14 G. Eda, H. Yamaguchi, D. Voiry, T. Fujita, M. Chen and M. Chhowalla, *Nano Lett.*, 2011, **11**, 5111-5116.
15 Z. Y. Zhao and Q. L. Liu, *Catal. Sci. Technol.*, 2018, **8**, 1867-1879.
16 D. Voiry, A. Goswami, R. Kappera, C. D. C. C. E. Silva, D. Kaplan, T. Fujita, M. Chen, T. Asefa and M. Chhowalla, *Nat. Chem.*, 2015, **7**, 45-49.
17 A. M. Van Der Zande, P. Y. Huang, D. A. Chenet, T. C. Berkelbach, Y. You, G. H. Lee, T. F. Heinz, D. R. Reichman, D. A. Muller and J. C. Hone, *Nat. Mater.*, 2013, **12**, 554-561.
18 S. Bertolazzi, M. Gobbi, Y. Zhao, C. Backes and P. Samorì, *Chem. Soc. Rev.*, 2018, **47**, 6845-6888.
19 B. L. Li, M. I. Setyawati, L. Chen, J. Xie, K. Ariga, C. T. Lim, S. Garaj and D. T. Leong, *ACS Appl. Mater. Interfaces*, 2017, **9**, 15286-15296.
20 S. S. Chou, M. De, J. Kim, S. Byun, C. Dykstra, J. Yu, J. Huang and V. P. Dravid, *J. Am. Chem. Soc.*, 2013, **135**, 4584-4587.
21 C. Backes, N. C. Berner, X. Chen, P. Lafargue, P. LaPlace, M. Freeley, G. S. Duesberg, J. N. Coleman and A. R. McDonald, *Angew. Chemie - Int. Ed.*, 2015, **23**, 2638-2642.
22 K. C. Knirsch, N. C. Berner, H. C. Nerl, C. S. Cucinotta, Z. Gholamvand, N. McEvoy, Z. Wang, I. Abramovic, P. Vecera, M. Halik, S. Sanvito, G. S. Duesberg, V. Nicolosi, F. Hauke, A. Hirsch, J. N. Coleman and C. Backes, *ACS Nano*, 2015, **9**, 6018-6030.
23 S. G. McAdams, E. A. Lewis, J. R. Brent, S. J. Haigh, A. G. Thomas, P. O'Brien, F. Tuna and D. J. Lewis, *Adv. Funct. Mater.*, 2017, **27**, 1703646.
24 S. Presolski and M. Pumera, *Mater. Today*, 2016, **19**, 140-145.
25 X. Chen and A. R. McDonald, *Adv. Mater.*, 2016, **28**, 5738-5746.
26 M. Vera-Hidalgo, E. Giovanelli, C. Navío and E. M. Pérez, *J. Am. Chem. Soc.*, 2019, **141**, 3767-3771.
27 M. Makarova, Y. Okawa and M. Aono, *J. Phys. Chem. C*, 2012, **116**, 22411-22416.
28 X. Chen, N. C. Berner, C. Backes, G. S. Duesberg and A. R. McDonald, *Angew. Chemie - Int. Ed.*, 2016, **55**, 5803-5808.
29 H. Pei**,** R. Sha, X. Wang, M. Zheng, C. Fan, J. W. Canary and N. C. Seeman, *J. Am. Chem. Soc.* 2019, **141**, 11923.
30 G.P. Acuna, F.M. Möller, P. Holzmeister, S. Beater, B. Lalkens and P. Tinnefeld, *Science*, **338**, 506-510.
31 K. Qu, J. Ren and X. Qu, *Mol. Biosyst.*, 2011, **7**, 2681-2687.
32 R. J. Macfarlane, B. Lee, M. R. Jones, N. Harris, G. C. Schatz and C. A. Mirkin, *Science* ,2011, **334**, 204-208.
33 A. Cecconello, L. V. Besteiro, A. O. Govorov and I. Willner, *Nat. Rev. Mater.*, 2017, **2**, 17039.
34 D. Huang, M. Freeley and M. Palma, *Sci. Rep.*, 2017, **7**, 45591.
35 D. Huang, K. Patel, S. Perez-Garrido, J. F. Marshall and M. Palma, *ACS Nano*, 2019, **13**, 728-736.
36 W. Hawkes, D. Huang, P. Reynolds, L. Hammond, M. Ward, N. Gadegaard, J. F. Marshall, T. Iskratsch and M. Palma, *Faraday Discuss.*, 2019, **219**, 203-219.

37 Q. Y. Lin, J. A. Mason, Z. Li, W. Zhou, M. N. O'Brien, K. A. Brown, M. R. Jones, S. Butun, B. Lee, V. P. Dravid, K. Aydin and C. A. Mirkin, *Science* ,2018, **359**, 669-672.

38 M. R. Jones, N. C. Seeman and C. A. Mirkin, *Science*, 2015, **347**, 1260901.

39 B. Yurke, A. J. Turberfield, A. P. Jr Mills, F. C. Simmel and J. L. Neumann, *Nature*, 2000, **406**, 605-608.

40 G. Amoroso, Q. Ye, K. Cervantes-Salguero, G. Fernández, A. Cecconello and M. Palma, *Chem. Mater.*, 2019, **31**, 1537-1542.

41 M. Freeley, A. Attanzio, A. Cecconello, G. Amoroso, P. Clement, G. Fernandez, F. Gesuele and M. Palma, *Adv. Sci.*, 2018, **5**, 1800596.

42 K. Gehring, J. L. Leroy and M. Guéron, *Nature*, 1993, **363**, 561-565.

43 F. C. Simmel, B. Yurke, H. R. Singh, *Chem. Rev.,* 2019, **119**, 6326-6369.